Photoionization cross sections for ions of the cerium isonuclear sequence

M. Habibi, D. A. Esteves, and R. A. Phaneuf
Department of Physics, University of Nevada, MS 220, Reno, Nevada 89557-0058, USA

A. L. D. Kilcoyne and A. Aguilar
Advanced Light Source, Lawrence Berkeley National Laboratory, MS 7-100, Berkeley, California 94720-8225, USA

C. Cisneros
Instituto de Ciencias Físicas, Universidad Nacional Autónoma de México, Apartado Postal 48-3, Cuernavaca, Morelos 62251, Mexico
(Received 9 June 2009; published 9 September 2009)

Photoionization cross sections for Ce^{q+} $(1 \leq q \leq 9)$ ions were measured in the 105–180 eV energy range of the $4d$ inner-shell giant resonance by merging a mass-to-charge-ratio-selected ion beam with a beam of monochromatized synchrotron radiation. The Cowan atomic structure code was used as an aid to interpret the experimental data. Four Rydberg series for $4d \rightarrow nf$ $(n \geq 4)$ and $4d \rightarrow np$ $(n \geq 6)$ autoionizing excitations were assigned using the quantum-defect theory in the Ce^{3+} photoionization cross section. The experimental data show the collapse of the nf wave functions $(n \geq 4)$ with increasing ionization stage as outer-shell electrons are stripped from the parent ion. The nf orbital collapse occurs partially for Ce^{2+} and Ce^{3+} ions and completely for Ce^{4+}, where these wave functions penetrate the core region of the ion. A strong contribution to the total oscillator strength was observed in multiple photoionization channels for Ce^{+}, Ce^{2+}, and Ce^{3+}, whereas most of the $4d$ excitations of the higher charge states decay by ejection of one electron.

DOI: 10.1103/PhysRevA.80.033407 PACS number(s): 32.80.Fb, 32.80.Aa, 32.70.Cs

I. INTRODUCTION

The experimental study of the nature and character of atoms and ions has always been a challenge for physicists. Photoionization experiments on multiply-charged ions are important as probes of electronic correlation and relativistic effects along isonuclear and isoelectronic series and provide data to benchmark atomic theory and models in plasma physics and astrophysics. Presented in this paper is an experimental investigation over a wide range of charge states of multiply-charged cerium ions. The focus of this investigation was photoionization processes involving $4d$ electrons along the isonuclear series of cerium ions. The objective was to provide as complete a picture as possible of the ion charge-state dependences of the observed features in the photon energy range of $4d$ electron excitation and ionization.

Photoionization data for members of the lanthanide group (atomic numbers Z from 57 to 71) are of increasing astrophysical interest in connection with studies of nucleosynthesis and star formation [1] since a considerable number of lines belong to the third spectrum (doubly-charged ions), corresponding to the dominant charge state in hot chemically peculiar stars [2]. Cowley reported in 1976 that cerium is the most abundant lanthanide element in the so-called Ap stars [2,3], which emit strong spectral lines of metallic elements.

Photoionization experiments on several isoelectronic and isonuclear sequences were conducted during the last 30 years to study systematics of electron correlation and relativistic effects in the photon energy region of $4d$ inner-shell excitation of atoms and atomic ions with different numbers of electrons in their outer shells. Photoionization cross-section measurements for Ba, Ba^{+}, and Ba^{2+} ions were performed by Lucatorto *et al.* at the National Bureau of Standards using the dual laser plasma (DLP) technique [4]. They concluded that most of the $4d$ absorption oscillator strengths of Ba and Ba^{+} are in the continuum, whereas the Ba^{2+} cross section is dominated by strong discrete transitions. Bizau *et al.* studied the Ba^{q+} $(q=2-6)$ and Xe^{q+} $(q=3-7)$ isonuclear sequences using a merged-beam technique at the SuperACO synchrotron light source in France and the Miyake undulator beamline in Denmark [5–10]. Their measurements indicate a dominance of discrete resonances for Ba^{4+}. O'Sullivan *et al.* measured the $4d$ photoabsorption of I^{q+} ions $(q=0-2)$ using the DLP technique [11], concluding that the dominant features arise from $4d \rightarrow \varepsilon f$ excitation manifested by a shape resonance in neutral iodine and from $4d \rightarrow nf$ discrete transitions in I^{2+}. The isonuclear sequence of Cs through Cs^{4+} was studied by Cummings *et al.* using the DLP technique [12]. Absolute photoionization cross-section measurements for Xe^{4+}, Xe^{5+}, and Xe^{6+} ions were performed at the Advanced Light Source (ALS) in Berkeley by Aguilar *et al.* [13] using the ion-photon merged-beams technique in support of the development of an extreme ultraviolet lithography light source at a wavelength of 13.5 nm.

Recently, photoionization of Ce encapsulated within the fullerene molecular ion C_{82}^{+} has been investigated by Müller *et al.* in the photon energy range of $4d$ excitations [14]. These measurements indicated a clear signature of excitation of the $4d$ subshell in both single and double ionizations of the $Ce@C_{82}^{+}$ endohedral fullerene molecular ion and verified the predicted +3 valency of the encaged Ce ion.

II. EXPERIMENTAL TECHNIQUE

Relative and absolute photoionization cross-section measurements were performed using the ion-photon-beam end station installed on undulator beamline 10.0.1 of the ALS. Cerium ions were produced by evaporating cerium metallocene $[(C_5H_5)_3Ce]$ into the plasma discharge of an electron-

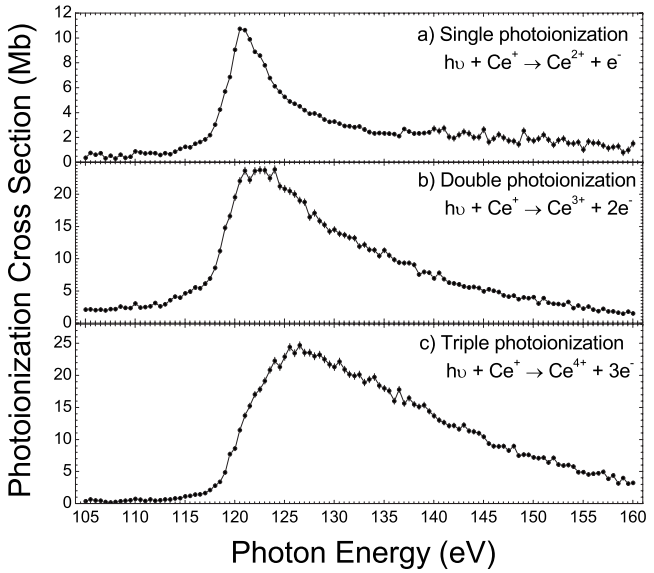

FIG. 1. (a) Single-, (b) double-, and (c) triple-photoionization cross sections of Ce^+ at a photon energy resolution of 0.1 eV.

cyclotron-resonance ion source and an ion beam was extracted by applying a potential of +4 or +6 kV to the source. A 60° dipole analyzing magnet selected ions of the desired momentum per charge. Following collimation and focusing, a spherical electrostatic deflector merged the ion beam onto the axis of a counterpropagating beam of monochromatized synchrotron radiation. After interacting with the photon beam over a common path of 1.4 m, the primary and product ion beams were demerged and separated by a 45° dipole magnet and independently collected by a Faraday cup and a single-particle detector, respectively. For spectroscopic measurements, the photoions were counted as the photon energy was changed in small steps at constant energy resolution. Absolute cross-section measurements were made at discrete photon energies under well-defined conditions, for which two-dimensional spatial intensity profiles of the photon and ion beams were carefully measured at three points within a central interaction region of known length (29.4 ± 0.6 cm). The total uncertainty of the cross-section measurements reported here is estimated to be $\pm 23\%$. Further details concerning the merged-beams apparatus and experimental method may be found in a previous report [15].

III. RESULTS

A. Photoionization of Ce^+

Figure 1 presents the measured cross sections for single, double, and triple photoionization of Ce^+. A broad asymmetric resonance dominates the cross sections in the energy range where $4d$ excitations are expected and extends to the $4d$ continuum. These features are attributed to $4d \rightarrow \varepsilon f$ transitions. The associated oscillator strengths determined by integrating the cross sections are presented in Table I. Within the experimental uncertainty, a total of 10.8 is consistent with the value of 10 for the $4d$ subshell predicted by the Thomas-Reiche-Kuhn sum rule.

TABLE I. Oscillator strengths (f) for single, double, and triple photoionization of La-like Ce^+.

Final charge state	Energy range (eV)	f	Partial contribution (%)
2	105–160	1.55	14.2
3	105–160	4.18	38.6
4	105–160	5.10	47.2
Total	105–160	10.8	100

Structure attributed to $4d \rightarrow np$ ($n \geq 6$) autoionizing excitations is evident in the single-photoionization cross section [Fig. 1(a)] above 135 eV with a small contribution to the total oscillator strength. So-called "satellite" transitions are likely present above the $4d$ ionization threshold corresponding to $4d$ ionization with excitation of one $4f$ or $5d$ electron or two $5d$ electrons [7,16]. However, their contribution to the total oscillator strength is very small.

Double photoionization [Fig. 1(b)] is attributed mostly to the $4d \rightarrow \varepsilon f$ ionization followed by single autoionization competing with multiple autoionization channels. A possible scheme for this process is

$$\gamma + Ce^+(4d^{10}4f5d^2) \rightarrow Ce^{2+(*)}(4d^9 4f5d^2) + e^-(\varepsilon) \hookrightarrow Ce^{3+}(4d^{10}5d) + 2e^-.$$

The weak resonant transitions present in the cross section below the $4d$ ionization threshold could be due to $4d \rightarrow nl$ ($n \geq 6$ and $l=1$ or $n \geq 4$ and $l=3$) excitations decaying by sequential ejection of two Auger electrons,

$$\gamma + Ce^+(4d^{10}5p^6 4f5d^2) \rightarrow Ce^{+(**)}(4d^9 5p^6 4f5d^2 nl) \hookrightarrow Ce^{2+(*)}(4d^{10}5p^5 4f5d^2) + e^- \hookrightarrow Ce^{3+}(4d^{10}5p^6 4f) + 2e^-.$$

Triple photoionization [Fig. 1(c)] is attributed mainly to direct $4d$ photoionization followed by the ejection of two sequential Auger electrons. Two autoionization paths are suggested for this process,

$$\gamma + Ce^+(4d^{10}5p^6 4f5d^2) \rightarrow Ce^{2+(**)}(4d^9 5p^6 4f5d^2) + e^-(\varepsilon) \hookrightarrow Ce^{3+(*)}(4d^{10}5p^5 5d^2) + 2e^- \hookrightarrow Ce^{4+}(4d^{10}5p^6) + 3e^-$$

or

$$\gamma + Ce^+(4d^{10}5s^2 5p^6 4f5d^2) \rightarrow Ce^{2+(**)}(4d^9 5s^2 5p^6 4f5d^2) + e^-(\varepsilon) \hookrightarrow Ce^{3+(*)}(4d^{10}5s5p^6 5d^2) + 2e^- \hookrightarrow Ce^{4+}(4d^{10}5s^2 5p^5 5d) + 3e^-.$$

The weak resonant structure in the cross section likely arises from excitation of a $4d$ electron to a higher energy state followed by ejection of three Auger electrons,

$$\gamma + \mathrm{Ce}^{+}(4d^{10}5s^{2}5p^{6}4f5d^{2})$$
$$\rightarrow \mathrm{Ce}^{+(***)}(4d^{9}5s^{2}5p^{6}4f5d^{2}nl)$$
$$\hookrightarrow \mathrm{Ce}^{2+(**)}(4d^{10}5s5p^{6}4f5d^{2}) + e^{-}$$
$$\hookrightarrow \mathrm{Ce}^{3+(*)}(4d^{10}5s^{2}5p^{5}4f5d) + 2e^{-}$$
$$\hookrightarrow \mathrm{Ce}^{4+}(4d^{10}5s^{2}5p^{6}) + 3e^{-}.$$

B. Photoionization of Ce^{2+}

Measured cross sections for single, double, and triple photoionization of Ce^{2+} are presented in Fig. 2 along with their associated oscillator strengths in Table II.

Discrete resonances due to autoionizing excitations of the $4d$ inner shell to $4f$ and np ($n \geq 6$) outer shells are evident in the single-photoionization cross section below 127.5 eV. Direct photoionization dominates above 127.5 eV, constituting 38% of the oscillator strength for this channel. Identification of $4d \rightarrow np$ Rydberg series was not possible due to the small oscillator strengths of these transitions compared to those of $4d \rightarrow 4f$ transitions.

A broad asymmetric shape resonance dominates the double-photoionization cross section where $4d$ excitations are expected and extends to the $4d$ continuum, similar to that observed in photoionization of Ce^{+}. This is attributed to $4d \rightarrow \varepsilon f$ direct photoionization accompanied by double autoionization. Resonant photoionization attributed to $4d \rightarrow 4f$ excitations followed by autoionization is evident in the cross section below 127 eV. Features due to $4d \rightarrow np$ autoionizing excitations may also be present but calculations indicated their contribution to the total oscillator strength to be relatively small.

The energy onset of the triple-photoionization cross section indicates a threshold of 123.5 ± 1.3 eV, which compares to 122.5 eV tabulated by NIST [17]. Possible weak resonant features likely result from excitation of the $4d$ electrons to higher energy states followed by emission of three Auger electrons. The oscillator strengths in Table II indicate the dominance of double photoionization, which constitutes more than half of the total photoionization oscillator strength of Ce^{2+} in this energy range. Since Auger decay of the $4d$ vacancy states dominates compared to radiative decay, the total oscillator strength in Table II is expected to correspond to the total for the $4d$ subshell. The measured value greater than 10 (the number of $4d$ electrons) is not surprising since direct photoionization of $5s$, $5p$, and $4f$ electrons is also possible in this energy range.

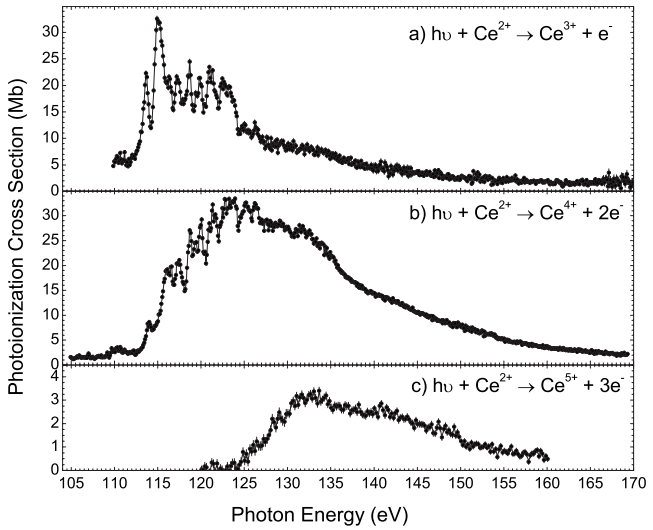

FIG. 2. (a) Single-, (b) double-, and (c) triple-photoionization cross sections of Ce^{2+} at a photon energy resolution of 0.1 eV.

C. Photoionization of Ce^{3+}

Single-photoionization cross section for Ce^{3+}, presented in Fig. 3(a), is dominated by $4d \rightarrow nf$ and $4d \rightarrow np$ autoionizing excitations. Two Rydberg series resulting from transitions of $4d$ electrons to excited nf and np orbitals were identified and assigned. Figure 4 presents two fits of the experimental resonance energies as functions of the principal quantum number by use of the quantum-defect form of the Rydberg formula,

$$E_n = E_{limit} - \frac{R_{\mathrm{Ce}}(Z - N_c)^2}{(n - \delta_n)^2}. \quad (1)$$

E_n is the transition energy, E_{limit} is the ionization potential of the electron being excited to the corresponding final state ($n = \infty$), Z is the nuclear charge, and N_c is the number of core electrons. The dimensionless quantum-defect parameter δ_n is a measure of the departure of the energy level E_n from a pure hydrogenic value ($\delta_n = 0$). The Rydberg constant R_{Ce} for cerium ions is given by

$$R_{\mathrm{Ce}} = \frac{\mu e^4}{4\pi\hbar c}, \quad (2)$$

where $\mu = (1/m_e + 1/M_{\mathrm{Ce}})^{-1}$ is the reduced mass of the electron-nucleus system of the cerium ion, e and m_e are the charge and the mass of the electron, respectively, $\hbar$ is the reduced Planck constant, and M_{Ce} is the mass of the cerium nucleus. In the present analysis, δ_n was replaced by a mean quantum-defect parameter δ for each Rydberg series.

The first Rydberg series is attributed to autoionizing excitations of Ce^{3+} in the ground state to $4d^{9}5s^{2}5p^{6}4f^{1}(^{1}F)nf^{1}\ ^{2}P_{3/2}$ ($n \geq 4$) states converging to the $4d^{9}5s^{2}5p^{6}4f^{1}\ ^{1}F$ limit of Ce^{4+}. The calculated energy limit (E_{limit}) for this series is 150.21 eV using the Cowan code [18–20], compared to the fit value of 150.48 eV using the quantum-defect theory. The second Rydberg series originates from $4d$ excitations of the $^{2}F^{o}_{7/2}$ metastable state to

TABLE II. Oscillator strengths (f) for single, double, and triple photoionization of Ba-like Ce^{2+}.

Final charge state	Energy range (eV)	f	Partial contribution (%)
3	110–173	4.04	33.4
4	105–169	7.47	61.7
5	120–160	0.59	4.9
Total		12.10	100.0

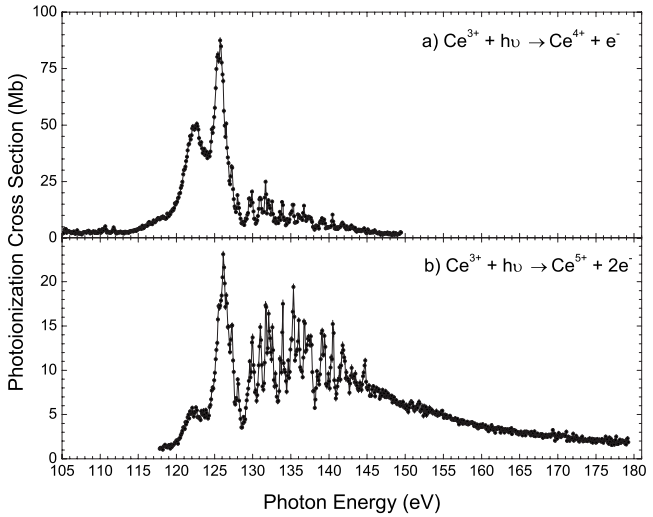

FIG. 3. (a) Single- and (b) double-photoionization cross sections of Ce^{3+} at a photon energy resolution of 0.1 eV.

$4d^9 5s^2 5p^6 4f^1 (^3H) np^1\ ^4G_{9/2}$ $(n \geq 6)$ states converging to the $4d^9 5s^2 5p^6 4f^1\ ^3H$ limit of Ce^{4+}. The energy limit of 143.33 eV of this series is in good agreement with the Cowan code calculated energy of 143.34 eV [18].

Figure 3(b) shows the double-photoionization cross-section measurements for Ce^{3+} from 105 to 180 eV photon energy at 0.1 eV resolution. Direct photoionization accompanied by autoionization dominates the cross section above 150 eV. This may be represented by the following process:

$$\gamma + Ce^{3+}(4d^{10}5s^2 5p^6 4f^1) \rightarrow Ce^{4+(*)}(4d^9 5s^2 5p^6 4f^1) + e^-$$
$$\hookrightarrow Ce^{5+}(4d^{10}5s^2 5p^5) + 2e^-.$$

Resonant photoionization cross-section features observed below 150 eV originate from $4d$ excitations to higher energy nf and np orbitals accompanied by emission of two Auger electrons. Two Rydberg series were assigned in the double-photoionization cross section of Ce^{3+}, both originating from the ground state. The corresponding energies and fits are indicated in Fig. 5 The first series results from excitation to the $4d^9 5s^2 5p^6 4f^1 (^1F) nf^1\ ^2P_{3/2}$ final state, which is identical to the first series observed in the single-photoionization cross section. An increase in the double-to-single-photoionization cross-section ratio for the higher members of this series at increasing photon energy indicates the competition between different autoionizing channels. The second Rydberg series arises from excitations to $4d^9 5s^2 5p^6 4f^1 (^1F) np^1\ ^2F_{5/2}$ final states. No identifications were made of Rydberg series due to double photoionization from metastable states.

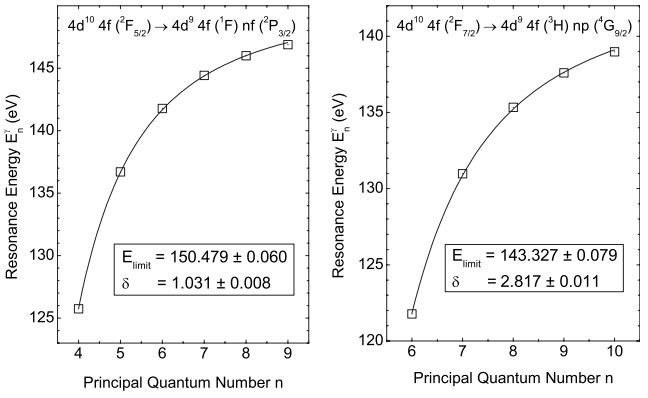

FIG. 4. Rydberg fits for the $4d^{10}4f^1 nf^1\ ^2P_{3/2}$ and $4d^{10}4f^1 np^1\ ^4G_{9/2}$ series originating from the $^2F_{5/2}$ ground state and the $^2F_{7/2}$ metastable state, respectively, in the single-photoionization cross section of Ce^{3+}. The series limit E_{limit} and quantum-defect parameter δ are given for each series.

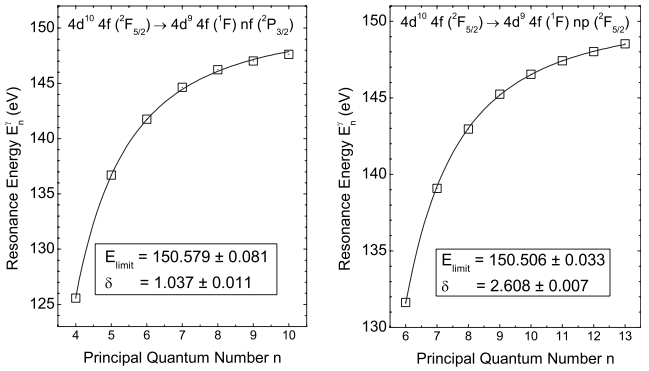

FIG. 5. Rydberg fits for the $4d^{10}4f^1 nf^1\ ^2P_{3/2}$ and $4d^{10}4f^1 np^1\ ^2F_{5/2}$ series originating from the $^2F_{5/2}$ ground state in the double-photoionization cross section of Ce^{3+}.

Oscillator strengths determined from the cross sections for single and double photoionization of Ce^{3+} are 5.03 and 3.64, respectively. Their sum of 8.67 is consistent with the expected value of 10 within the experimental uncertainty.

D. Photoionization of Ce^{4+}

Figure 6 shows the single-photoionization cross section of Ce^{4+} in the $4d$ inner-shell excitation region. The structure below 129.6 eV is attributed mostly to $4d^{10}5s^2 5p^5 4f \rightarrow 4d^9 5s^2 5p^5 4f^2$ transitions followed by ejection of an Auger electron. The features are very broad below 126 eV. Direct photoionization of the $5s^2$ subshell is also possible in this energy region, although its contribution to the total cross section is relatively small. The strongest resonance at 131.09 eV is assigned to $4d^{10}5p^6\ ^1S_0 \rightarrow 4d^9 5p^6 (4f\ ^2F)^3 D_1$ excitation followed by autoionization. Resonances near and including the strongest feature (129.7–135 eV) are attributed to unresolved fine structure of the final states of the $4d^9 5p^6 4f$ configuration. The structures at 136.52 and 139.09 eV are assigned to $4d \rightarrow 6p$ excitation from the ground state. The first is attributed to the $4d^9 5p^6 (6p\ ^2P)^1 P_1$ final state and the second to $4d^9 5p^6 (6p\ ^2P)^3 P_j$ final states. The measured energy splitting between the $^1P_1$ and $^3P_1$ fine states is 2.57 eV, which compares to a calculated value of 2.65 eV. At this energy resolution, the first resonance appears more symmetric than the second due to the hyperfine structure splittings in the latter, which is evident in measurements performed at higher photon energy resolution (not shown). The structures near 144.6 and 148 eV arise from the transitions $4d^{10}5p^6\ ^1S_0 \rightarrow 4d^9 5p^6 (5f\ ^2F)^3 D_j$ and $4d^{10}5p^6\ ^1S_0 \rightarrow 4d^9 5p^6 (5f\ ^2F)^1 P_1$, respectively. The measured splitting of

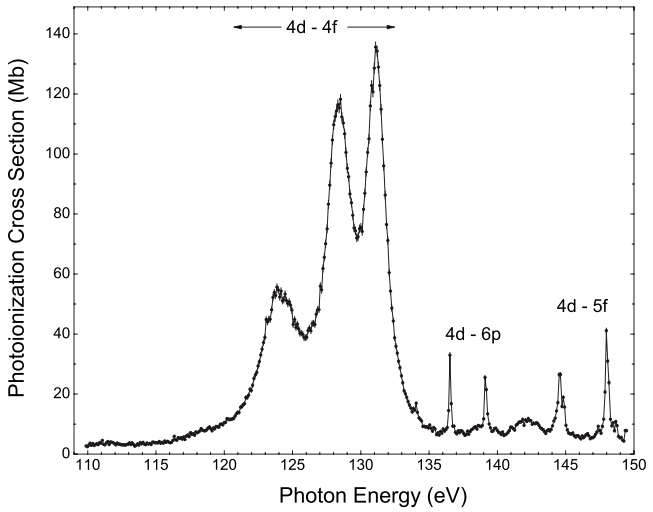

FIG. 6. Single-photoionization cross section of Ce^{4+} at a photon energy resolution of 0.1 eV.

the fine-structure states $^3D_1$ and $^1P_1$ is 3.5 eV compared to 3.4 eV in the calculations. Hyperfine structure is observed in the $^3D_1$ peak. The measured energy splitting between the $^3D_1$ and $^3D_3$ states is 0.27 eV, compared to a calculated value of 0.42 eV. A small resonance near the $^1P_1$ peak at 148.7 eV is attributed to excitation of $4d$ electrons from the ground state to $4d^9 5p^6(7p\ ^2P)^1P_1$.

The total oscillator strength determined from the measurements in this energy range is 10.32, consistent with the expected value of 10 for the $4d$ subshell.

E. Photoionization of Ce^{5+}

Figure 7(a) shows the absolute photoionization cross section measurements for Ce^{5+}. The total experimental oscillator strength is 10.77, which is in agreement with the sum-rule value of 10 within the experimental uncertainty. The structure above 131 eV arises mostly from $4d \rightarrow 4f$ excitation from the $^2P_{3/2}$ ground state and from the $^2P_{1/2}$ metastable

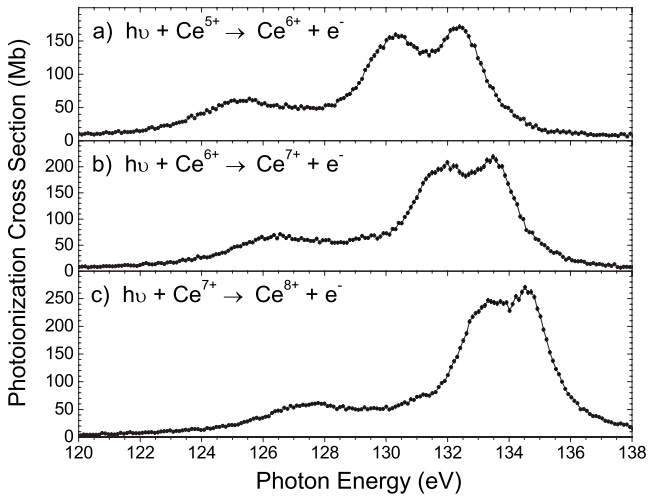

FIG. 7. Single-photoionization cross sections of (a) Ce^{5+}, (b) Ce^{6+}, and (c) Ce^{7+} at a photon energy resolution of 0.1 eV.

state, followed by autoionization. Features below 131 eV are attributed to $4d \rightarrow 4f$ excitation from the $4d^{10}5s^25p^44f$ metastable states of Ce^{5+} followed by autoionization. The measurements suggest that these autoionizing decays occur very rapidly, yielding broad resonances.

F. Photoionization of Ce^{6+}

Absolute photoionization cross-section measurements for Ce^{6+} are presented in Fig. 7(b). Above 132.5 eV, the measured structures are dominated by $4d \rightarrow 4f$ transitions from the ground-state $^3P_2$ and from the metastable states $^3P_0$, $^3P_1$, $^1D_2$, and $^1S_0$, followed by autoionization. The structures observed in the range from 115 to 132.5 eV are attributed mainly to $4d \rightarrow 4f$ excitation from the $4d^{10}5s^25p^34f$ metastable states of Ce^{6+}, followed by autoionization. The relative contributions of these metastable states to the total measured photoionization oscillator strength of Ce^{6+}(11.4) depend on their proportions in the primary ion beam. For photoionization of a pure ground-state Ce^{6+} ion beam, only the broad resonance peak centered near 133.5 eV would be expected.

G. Photoionization of Ce^{7+}

Figure 7(c) shows the measured photoionization cross section of Ce^{7+}. The structure observed below 128.5 eV is dominated by autoionizing excitations of $4d$ electrons from the $4d^{10}5s^25p^24f$ metastable states to $4d^95s^25p^24f^2$ excited states. Resonances in the energy range of 128.5–134 eV are attributed to $4d \rightarrow 4f$ transitions arising from an admixture of the ground state and metastable states. Above 134 eV, the structures are assigned to $4d \rightarrow 4f$ excitations from the $^4S_{3/2}$ ground state and $^2D_{3/2}$, $^2D_{5/2}$, $^2P_{1/2}$, and $^2P_{3/2}$ metastable states. The measured photoionization oscillator strength for Ce^{7+} is 12.23, which is consistent with the expected value of 10 within the estimated experimental uncertainty of $\pm 23\%$.

H. Photoionization of Ce^{8+}

Small resonant features observed in the photoionization cross section of Ce^{8+} (Fig. 8) below 127 eV are attributed to $5s \rightarrow np$ $(n \geq 8)$ transitions. A small step in the cross section near 125 eV corresponds to the opening of the $5p$ direct photoionization channel from the $^3P_0$ ground state. The step near 122 eV corresponds to the photoionization threshold of the $^3P_2$ metastable state, which lies 3.64 eV above the ground state [18]. However, accurate values of these thresholds could not be determined due to resonances embedded in the cross section in this energy range. Features in the energy range of 127–135.5 eV are attributed to $4d \rightarrow 4f$ transitions from an admixture of the ground state and metastable states, followed by autoionization. The features above 135.5 eV, including the strongest narrow resonance at 135.96 eV, are assigned to autoionizing $4d \rightarrow 4f$ excitations from the $^3P_0$ ground state and the $^3P_1$, $^3P_2$, $^1D_2$, and $^1S_0$ metastable levels of the ground-state configuration. Contributions of direct $5s$ photoionization from the ground state and metastable states are expected above 138 eV [18]. The integrated experimental oscillator strength in the energy range of these measurements is 12.45. A value larger than 10 is to be expected in this case

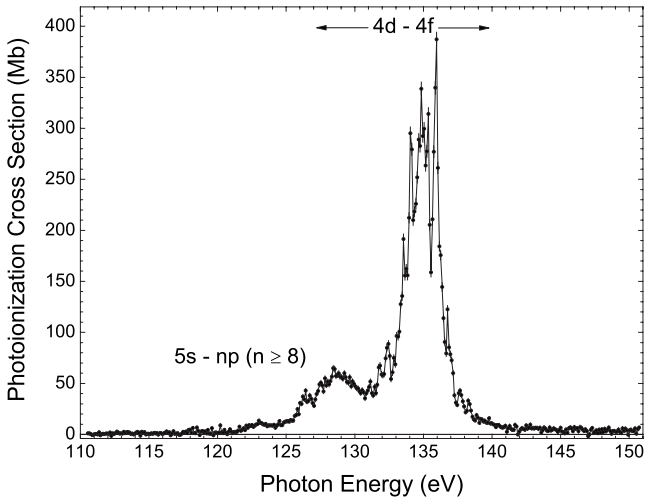

FIG. 8. Single-photoionization cross section of Ce^{8+} at a photon energy resolution of 0.1 eV.

because of direct and resonant contributions to the photoionization cross section from the 5*s* and 5*p* subshells in this energy range.

I. Photoionization of Ce^{9+}

Photoionization of Ce^{9+} (Fig. 9) shows little evidence for a direct photoionization threshold from the ground state, which is calculated to occur near 140.83 eV [18]. Therefore, no structure arising due to 4*d* excitation from the ground state was expected in this energy range. A small step in the cross section near 134.1 eV is attributed to the photoionization threshold of the $4d^{10}5s^24f^1\ ^2F_{5/2}$ metastable state, which is close to the calculated value of 133.63 eV [18]. The strong resonances above this threshold up to 136.8 eV are mostly attributed to $4d \rightarrow 4f$ and $4d \rightarrow np$ $(n=5,6)$ autoionizing excitations from the $^2F_{5/2}$ metastable state, although specific spectroscopic assignments were not made. A possible small step in the photoionization cross section near 136.8 eV might

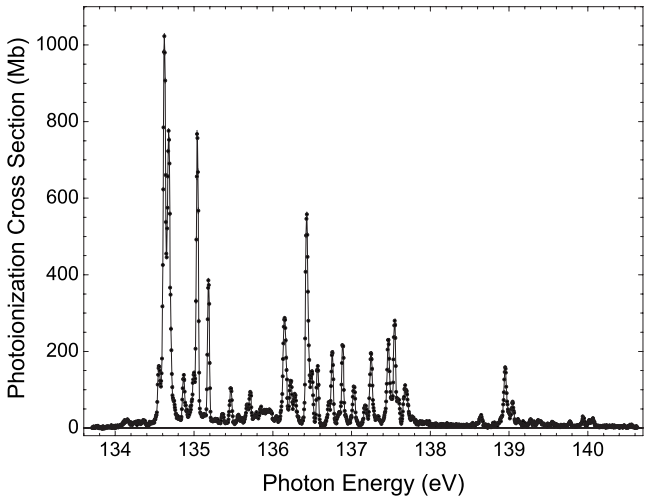

FIG. 9. Single-photoionization cross section of Ce^{9+} at a photon energy resolution of 0.05 eV.

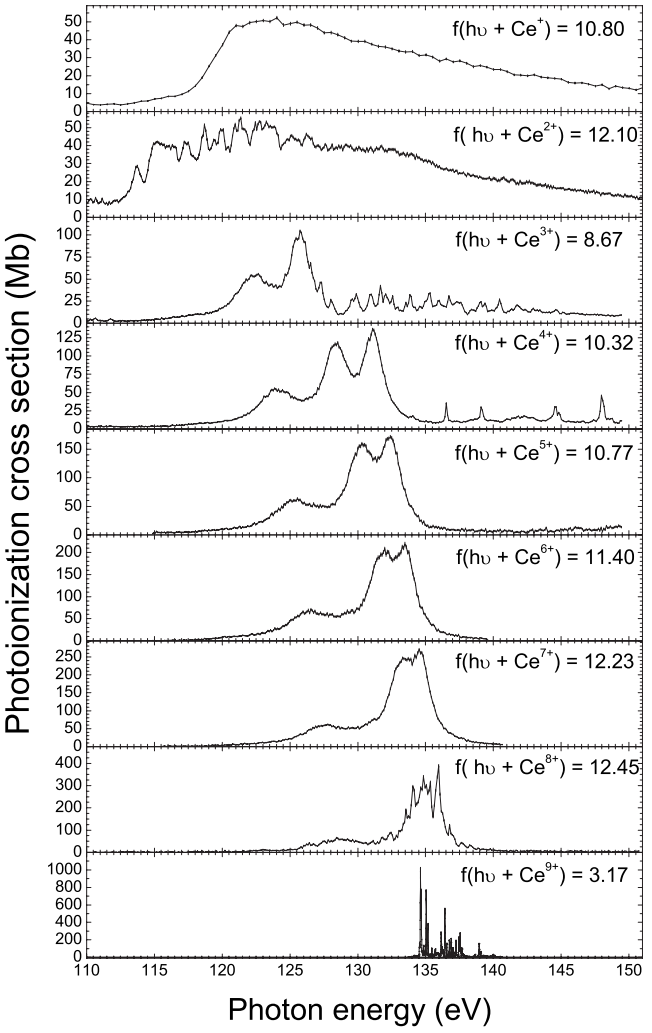

FIG. 10. Total photoionization cross sections for the cerium isonuclear sequence from Ce^+ through Ce^{9+} with their total measured oscillator strengths *f*. Double and triple photoionization are included in the total cross sections for those charge states for which they are energetically allowed in this energy range.

be due to the onset of direct photoionization of the $4d^{10}5s^25p^1\ ^2P_{3/2}$ metastable state, for which the calculated ionization potential is 136.82 eV [18]. The resonance features above 136.8 eV are assigned to autoionizing excitations of 4*d* electrons to 4*f*, 5*p*, and 6*p* from the $4d^{10}5s^25p^1\ ^2P_{3/2}$ metastable state. However, spectroscopic assignments of individual resonance features using the online version of the Cowan code were not possible.

Integration of the photoionization cross section of Ce^{9+} in the energy range of 133.7–140.6 eV yields an oscillator strength of 3.17. Since the ionization threshold of the ground state is close to 140.83 eV, the measured photoionization cross section in this energy range originates exclusively from the metastable states. Thus their proportion in the parent ion beam is estimated to be approximately 1/3.

IV. SUMMARY AND CONCLUSIONS

Photoionization cross sections for ions of the cerium isonuclear sequence from Ce^+ through Ce^{9+} were investigated

by an ion-photon merged-beam technique using monochromatized synchrotron radiation. Competition between continuum and discrete electronic transitions from the filled $4d$ subshell was observed along this ionic sequence, supporting the theoretical predictions for the collapse of the nf orbitals with increasing initial ion charge. Metastable states were present in all the parent ion beams, which complicated the analysis of the measured cross sections. Fractions of the primary ion beams in metastable states were estimated to be 1/4 for Ce^{4+} and 1/3 for Ce^{9+}. Figure 10 compares the total photoionization cross-section measurements for Ce^{+} through Ce^{9+} ions and their associated oscillator strengths in the photon energy range of $4d$ excitations. A broad asymmetric resonance dominates the cross section of Ce^{+}, whereas the cross section of Ce^{2+} is characterized by strong resonances below the $4d$ threshold and a delayed onset of direct photoionization. The Ce^{2+} cross section due to continuum excitation of the $4d$ subshell decreases monotonically at high energies. Strong and broad features dominate the cross section of Ce^{3+}, which also exhibits narrow but weaker resonances. The direct photoionization cross section of Ce^{3+} is much smaller than that for Ce^{+} and Ce^{2+}, indicating a growing competition between discrete and continuum photoionization processes with increasing ionization stage. Four Rydberg series were assigned in the single and double photoionization of Ce^{3+} arising from $4d \rightarrow nf$ and $4d \rightarrow np$ transitions. In the Ce^{4+} cross section, the direct photoionization is almost negligible and only discrete transitions are observed, which is the case for all the higher charge states. That indicates the "collapse" of the nf wave functions [21,22] into the inner well of the Coulomb potential that binds the electrons of the $4d$ subshell. This is a consequence of nuclear attraction dominating over the screening effect due to electron-electron interactions. In the case of Ce^{8+}, strong narrow resonances arising from $4d \rightarrow 4f$ autoionizing excitations dominate the photoionization cross section. Direct and indirect photoionization of the $5s$ and $5p$ subshells are also evident in the Ce^{6+}, Ce^{7+}, and Ce^{8+} cross sections, which account for the higher oscillator strengths in the experimental energy range for these ions. The Ce^{9+} cross section is dominated by more slowly autoionizing excitations of the $4d$ electrons originating exclusively from the metastable states of this ion since $4d$ excitation from the ground state populates only bound states.

ACKNOWLEDGMENTS

The authors are grateful to Dr. Ulyana Safronova for helpful discussions concerning the electronic structure of these ions and for identifications of metastable states. This research was supported by the U.S. Department of Energy, Division of Chemical Sciences, Biosciences, and Geosciences under Grant No. DOE-FG02-03ER15424.

[1] E. Biémont and P. Quinet, Phys. Scr. **T105**, 38 (2003).
[2] E. Biémont, P. Quinet, and T. A. Ryabchikova, Mon. Not. R. Astron. Soc. **336**, 1155 (2002).
[3] C. R. Cowley, Astrophys. J., Suppl. Ser. **32**, 631 (1976).
[4] T. B. Lucatorto, T. J. McIlrath, J. Sugar, and S. M. Younger, Phys. Rev. Lett. **47**, 1124 (1981).
[5] J. M. Bizau, D. Cubaynes, J. M. Esteva, F. J. Wuilleumier, C. Blancard, J. Bruneau, J. P. Champeaux, A. Compant LaFontaine, C. Couillaud, R. Marmoret, C. Rémond, D. Hitz, M. Delaunay, N. Haque, P. C. Deshmukh, H. L. Zhou, and S. T. Manson, Phys. Rev. Lett. **87**, 273002 (2001).
[6] J. M. Bizau, D. Cubaynes, M. Richter, F. J. Wuilleumier, J. Obert, J. C. Putaux, T. J. Morgan, E. Källne, S. Sorensen, and A. Damany, Phys. Rev. Lett. **67**, 576 (1991).
[7] J. M. Bizau, D. Cubaynes, P. Gérard, and F. J. Wuilleumier, Phys. Rev. A **40**, 3002 (1989).
[8] J. M. Bizau, J. M. Esteva, D. Cubaynes, F. J. Wuilleumier, C. Blancard, A. C. LaFontaine, C. Couillaud, J. Lachkar, R. Marmoret, C. Rémond, J. Bruneau, D. Hitz, P. Ludwig, and M. Delaunay, Phys. Rev. Lett. **84**, 435 (2000).
[9] J. M. Bizau, C. Blancard, D. Cubaynes, F. Folkmann, J. P. Champeaux, J. L. Lemaire, and F. J. Wuilleumier, Phys. Rev. A **73**, 022718 (2006).
[10] J. M. Bizau, E. Bouisset, C. Blancard, J. P. Champeaux, A. Compant la Fontaine, C. Couillaud, D. Cubaynes, D. Hitz, C. Vinsot, and F. J. Wuilleumier, Nucl. Instrum. Methods Phys. Res. B **205**, 290 (2003).
[11] G. O'Sullivan, C. McGuinness, J. T. Costello, E. T. Kennedy, and B. Weinmann, Phys. Rev. A **53**, 3211 (1996).
[12] A. Cummings, C. McGuinness, G. O'Sullivan, J. T. Costello, J. P. Mosnier, and E. T. Kennedy, Phys. Rev. A **63**, 022702 (2001).
[13] A. Aguilar, J. D. Gillaspy, G. F. Gribakin, R. A. Phaneuf, M. F. Gharaibeh, M. G. Kozlov, J. D. Bozek, and A. L. D. Kilcoyne, Phys. Rev. A **73**, 032717 (2006).
[14] A. Müller, S. Schippers, M. Habibi, D. Esteves, J. C. Wang, R. A. Phaneuf, A. L. D. Kilcoyne, A. Aguilar, and L. Dunsch, Phys. Rev. Lett. **101**, 133001 (2008).
[15] A. M. Covington, A. Aguilar, I. R. Covington, M. F. Gharaibeh, G. Hinojosa, C. A. Shirley, R. A. Phaneuf, I. Álvarez, C. Cisneros, I. Dominguez-Lopez, M. M. Sant'Anna, A. S. Schlachter, B. M. McLaughlin, and A. Dalgarno, Phys. Rev. A **66**, 062710 (2002).
[16] H. Kjeldsen, P. Andersen, F. Folkman, J. E. Hansen, M. Kitajima, and T. Andersen, J. Phys. B **35**, 2845 (2002).
[17] Yu. Ralchenko, A. E. Kramida, J. Reader, and NIST ASD Team, NIST Atomic Spectra Database, Version 3.1.5, 2008, http://physics.nist.gov/PhysRefData/ASD/index.html
[18] R. D. Cowan, Cowan Atomic Structure Code, http://aphysics2.lanl.gov/cgi-bin/ION/runlanl.pl
[19] R. D. Cowan, J. Opt. Soc. Am. **58**, 808 (1968).
[20] R. D. Cowan, *The Theory of Atomic Structure and Spectra* (University of California Press, Berkeley, CA, 1981).
[21] K. T. Cheng and C. Froese Fischer, Phys. Rev. A **28**, 2811 (1983).
[22] K. T. Cheng and W. R. Johnson, Phys. Rev. A **28**, 2820 (1983).